DRAFT VERSION MARCH 20, 2014
Preprint typeset using LaTeX style emulateapj v. 5/2/11

arXiv:1403.4905v1 [astro-ph.GA] 19 Mar 2014

DIFFUSE EXTRAPLANAR DUST IN NGC 891

KWANG-IL SEON[1,2], ADOLF N. WITT[3], JONG-HO SHINN[1], AND IL-JOONG KIM[1]

Draft version March 20, 2014

Abstract

We report the detection of vertically extended far-ultraviolet (FUV) and near-UV emissions in an edge-on spiral galaxy NGC 891, which we interpret as being due to dust-scattered starlight. Three-dimensional radiative transfer models are used to investigate the content of the extraplanar dust that is required to explain the UV emission. The UV halos are well reproduced by a radiative transfer model with two exponential dust disks, one with a scaleheight of $\approx 0.2-0.25$ kpc and the other with a scaleheight of $\approx 1.2-2.0$ kpc. The central face-on optical depth of the geometrically thick disk is found to be $\tau_B^{\rm thick} \approx 0.3-0.5$ at B-band. The results indicate that the dust mass at $|z| > 2$ kpc is $\approx 3-5\%$ of the total dust mass, which accord well with the recent Herschel sub-millimeter observation. Our results, together with the recent discovery of the UV halos in other edge-on galaxies, suggest the widespread existence of the geometrically thick dust layer above the galactic plane in spirals.

Subject headings: galaxies: halos — dust, extinction — radiative transfer — ultraviolet: galaxies

1. INTRODUCTION

The three-dimensional structure and the amount of dust in galaxies are of great importance in understanding galaxy evolution processes such as star formation. The dust content has been inferred from the radiative transfer models of the dust attenuation in optical/near-infrared (NIR) images of edge-on galaxies (Kylafis & Bahcall 1987; Byun et al. 1994; Kuchinski et al. 1998; Xilouris et al. 1997, 1998, 1999; De Looze et al. 2012). The absorbed energy by dust is re-emitted in far-IR (FIR)/sub-millimeter (submm) wavelengths, and thus FIR/submm observations provide another way to derive the dust content. However, it has been revealed that the spectral energy distribution (SED) in FIR/submm requires at least a dust mass twice as large as estimated from the radiative transfer model of optical/NIR images (Popescu et al. 2000; Misiriotis et al. 2001; Bianchi 2008; Baes et al. 2010; De Looze et al. 2012). To resolve the discrepancy, an extra dust mass in the form of a secondary thin disk + clumpy dust clouds associated with molecular clouds that was supposed to be hidden in optical images was introduced (Popescu et al. 2000; Tuffs et al. 2004; Misiriotis et al. 2004; Bianchi 2008; Popescu et al. 2011).

We note that the previous radiative models assumed the geometrically thin dust disk that is concentrated in the galactic midplane ($z = 0$). It may therefore be worthwhile to examine an additional dust component that is existing in a form different from the thin disk. In fact, there have been various attempts to investigate the existence of dust residing outside the galactic plane. Filamentary dust structures above the galactic plane have been observed up to $|z| \lesssim 2$ kpc in nearby edge-on spiral galaxies using high-resolution optical images (Howk & Savage 1997; Alton et al. 2000a; Rossa et al. 2004; Thompson et al. 2004). The extraplanar dust filaments were found to contain too small an amount of dust ($\sim 1-2\%$ of the total dust mass) to be considered as the additional dust component (Popescu et al. 2000). The filamentary features, however, were traced in absorption against the background starlight, thereby implying preferentially "dense" dust features visible only to heights limited by the vertical extent of the background starlight. Therefore, "diffuse" dust component above the galactic plane was not traceable in the studies.

We searched the diffuse extraplanar dust based on the fact that the dust should appear as a faint extended reflection nebula illuminated by starlight. The scattered light would not be easily distinguished from direct starlight when the scaleheight of the light source is greater than or comparable to that of the extraplanar dust. Therefore, far-ultraviolet (FUV) and/or near-UV (NUV) observation of edge-on galaxies can provide the best method for detecting the scattered light from the diffuse extraplanar dust, because OB stars, the main source of the UV continuum, have a scaleheight < 0.2 kpc and have no bulge or halo component. We thus examined the UV data of the edge-on galaxies obtained from the *Galaxy Evolution Explorer (GALEX)* mission. The discovery of the UV halos due to the diffuse dust existing above the galactic plane of NGC 891 was first reported in Seon & Witt (2012a). Hodges-Kluck & Bregman (2014) describe the discovery of the UV halos around many galaxies, including NGC 891. In this Letter, we use a radiative transfer model to study the content of the extended UV emission in NGC 891.

2. DATA ANALYSIS

We used the archival FUV and NUV data set "GI2_019004_3C66B_22013" of the *GALEX* mission (Morrissey et al. 2007) to study the diffuse extraplanar dust of the most studied nearby edge-on spiral galaxy NGC 891. Fig. 1 shows the FUV and NUV images and contours, together with the radial and vertical intensity profiles of NGC 891. Foreground bright stars were masked in the images. It is clear that the FUV and NUV emissions are extended not only along the major axis, but also in the direction of the minor axis. The NUV image is more extended than the FUV image along the major axis. The backgrounds were subtracted as in the following paragraph. We note a large asymmetry between the northeast (NE; $x < 0$; left) and the southwest (SW; $x > 0$; right) sides at the midplane, which has been noted also in H I (Oosterloo et al. 2007), Hα (Rand et al. 1990), and optical

[1] Korea Astronomy and Space Science Institute, Daejeon, 305-348, Korea; E-mail: kiseon@kasi.re.kr
[2] Astronomy and Space Science Major, University of Science & Technology, Daejeon, 305-350, Korea
[3] Ritter Astrophysical Research Center, University of Toledo, Toledo, OH 43606, USA

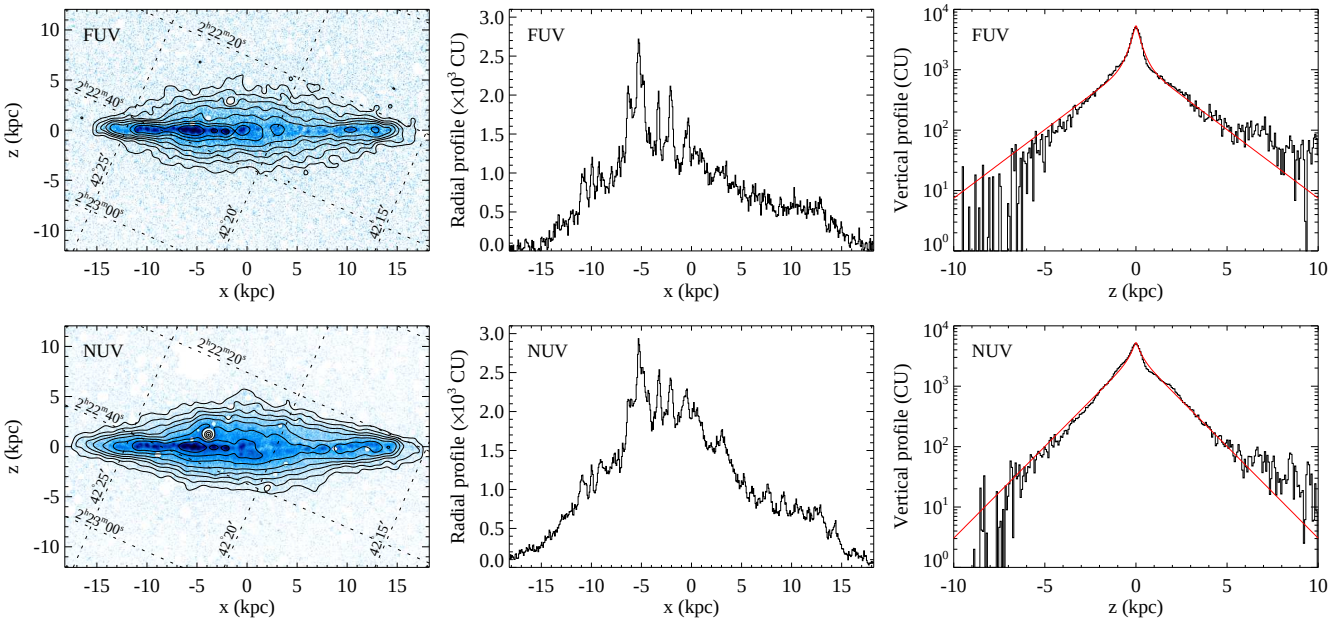

Figure 1. *GALEX* maps and intensity profiles of NGC 891. The images were rotated such that the major axis of the disk is horizontal and scaled as asinh. Contour levels correspond to I = 250, 450, 700, 1000, 1500, 2500, 4000, and 7000 photons cm^{-2} s^{-1} sr^{-1} Å^{-1}(continuum unit; CU) above the background intensity. The contours were made after smoothing the images by a Gaussian function with full width at half maximum (FWHM) of 10 pixels (corresponding to 0.7 kpc). However, the displayed images were not smoothed. Concentric contours and white regions are artifacts due to the masking of foreground stars. A distance of 9.5 Mpc to NGC 891 was assumed. Black solid lines represent the observed profiles. The red curves are the best-fit two-exponential functions for the vertical profiles. The vertical profiles were obtained by averaging over the whole disk and the radial profiles over $|z| < 5$ kpc.

images (Xilouris et al. 1998). The asymmetry is consistent with the idea of a trailing spiral structure with the dust behind OB stars and the fact that the SW side is the receding side (van der Kruit & Searle 1981; Kamphuis et al. 2007). Therefore, the starlight from the SW side would have been almost completely obscured by the dust. The FUV emission is more radially extended in the SW side than in the NE side. The vertical profiles show a core and an extended tail. In addition, the vertical features show general correlations with star forming regions in the midplane. The north ($z > 0$) side from the midplane is more vertically extended than the south ($z < 0$) side in both wavelength bands. The tail component of the north side flattens while in the south side becomes less extended. However, the excess at $z \gtrsim 6$ kpc is not statistically significant.

We fitted the average vertical intensity profiles over the whole disk with two exponential functions and a constant, and then subtracted the best-fit backgrounds from the data. The background levels were estimated ~ 1465 and ~ 1995 photons cm^{-2} s^{-1} sr^{-1} Å^{-1} (continuum unit, hereafter CU) for the FUV and NUV data, respectively. The background values are consistent with those of Gil de Paz et al. (2007), which were estimated by using the data set with less exposure time. The UV background in our Galaxy is mostly caused by the dust scattering of starlight (Witt et al. 1997; Seon et al. 2011; Hamden et al. 2013). Using Eq. (10) of Seon et al. (2011), which were derived from the FUV background observation of our Galaxy, we obtain the FUV background of ~ 1400 CU at the Galactic latitude of NGC 891. Therefore, the estimated background is consistent with the FUV background observation.

The average vertical profiles over the whole disk are well fitted by $4.4e^{-|z|/0.29} + 1.4e^{-|z|/1.91}$ ($\times 10^3$) and $2.3e^{-|z|/0.26} + 3.3e^{-|z|/1.43}$ ($\times 10^3$) CU for the FUV and NUV data, respectively. The best-fit profiles are shown in Fig. 1. We note that the point spread function (PSF) of GALEX is approximately Gaussian with an extended wing at large radii. However, the extended wing is too small to account for the extended UV profile. The full width at half maximum (FWHM) of the PSF is $\sim 4.2''$ and $\sim 5.3''$ for the FUV and NUV bands, respectively, corresponding to 0.19 and 0.24 kpc at the distance to NGC 891 (Gil de Paz et al. 2007; van der Kruit & Searle 1981; Morrissey et al. 2007), and thereby the true scaleheights of the core components should be smaller than the best-fit values.

3. RADIATIVE TRANSFER MODEL

To find the dust distribution, radiative transfer models of the dust-scattered FUV radiation were calculated using a three-dimensional Monte-Carlo simulation code (Lee et al. 2008; Seon 2009; Seon & Witt 2012b, 2013). The code models multiple scattering of photons and use a scheme that includes "forced first scattering" to improve the calculation efficiency in optically thin medium and a "peeling-off" technique to produce an image toward the observer.

The radiative transfer calculations adopt smooth axisymmetric models for the dust and illuminating starlight. We assume that both the stars and the dust are exponentially distributed not only in the direction perpendicular to the galactic plane but also in the radial direction. The models with a single exponential dust disk were obviously not able to produce the vertical profile of the data. The extended tails in the vertical profiles suggest a geometrically thick dust component. Therefore, we added one more exponential dust disk. Then, the extinction coefficient due to two exponential dust disks is given by

$$\kappa(r,z) = \kappa_0^{\rm thin} \exp\left(-\frac{r}{h_d^{\rm thin}} - \frac{|z|}{z_d^{\rm thin}}\right) + \kappa_0^{\rm thick} \exp\left(-\frac{r}{h_d^{\rm thick}} - \frac{|z|}{z_d^{\rm thick}}\right),$$

where r and z are cylindrical coordinates. Here, $h_d^{\rm thin}$ and $z_d^{\rm thin}$ are the scalelength and scaleheight of the geometrically thin

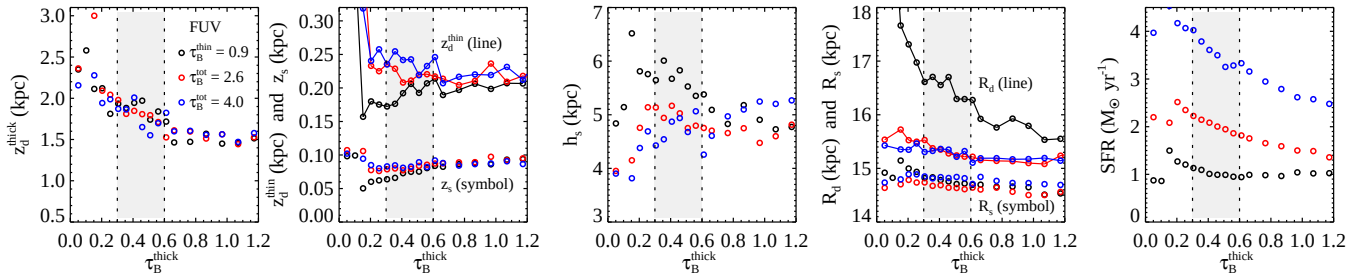

Figure 2. Best-fit parameters versus τ_B^{thick} for each model type. From left to right panels are shown the scaleheights (z_d^{thick}, z_d^{thin}, z_s) of the dust and stellar disks, the scalelength (h_s) of stellar disk, the maximum radial extents (R_d, R_s) of the dust and stellar disks, and the star formation rate inferred from the stellar luminosity. Black, red and blue colors represent the model types that assume τ_B^{thin} = 0.9, τ_B^{tot} = 2.6, and τ_B^{tot} = 4, respectively.

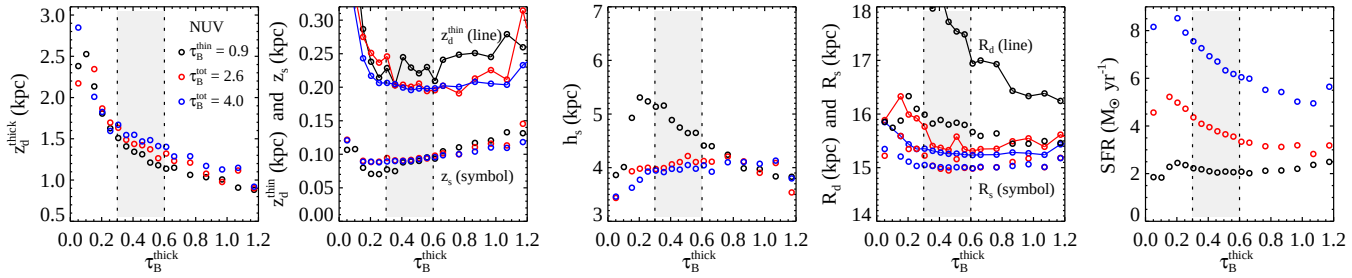

Figure 3. Same as Figure 2, but for the NUV data

dust disk, respectively, and h_d^{thick} and z_d^{thick} of the geometrically thick disk. κ_0^{thin} and κ_0^{thick} are the extinction coefficients at the center of disks. The central optical depth of the model galaxy seen face-on is then given by $\tau = \tau^{thin} + \tau^{thick} = 2\kappa_0^{thin} z_d^{thin} + 2\kappa_0^{thick} z_d^{thick}$. The starlight is given by

$$I(r,z) = I_0 \exp\left(-\frac{r}{h_s} - \frac{|z|}{z_s}\right),$$

where h_s and z_s are the scalelength and scaleheight of the young stars, respectively. The stellar disk was truncated at R_s, and the dust disks were truncated at R_d along the radial direction. Anisotropy parameters and albedos at the FUV and NUV wavelengths were adopted from the Milky Way dust properties (Draine 2003). The instrumental PSFs were then convolved with the models. Because our models are azimuthally symmetric, we folded the observed images about the minor axis, as in Xilouris et al. (1997, 1998, 1999), so that the fitted galaxy is an average of the left and right halves of the galaxy.

We attempted to perform a detailed parameter fit to the data through the χ^2 minimization technique. However, the model parameters could not be constrained simultaneously. We therefore adopted the spatial distribution of a thin dust disk similar to the results of Xilouris et al. (1998, 1999). As the thick disk seems to be closely related to the activities in the galactic plane, the thick disk was assumed to have the same scalelength as the thin disk, i.e., $h_d^{thin} = h_d^{thick} = 8$ kpc. We also assumed the inclination angle $\theta = 89.8^\circ$ and a distance of 9.5 Mpc to NGC 891 (van der Kruit & Searle 1981; Xilouris et al. 1998).

Three kinds of models were attempted. In the first type, the face-on optical depth for the thin disk is assumed to be τ_B^{thin} = 0.9 in B-band (τ_{FUV}^{thin} = 1.8 in FUV-band), motivated by the optical observations (Xilouris et al. 1998, 1999). However, the FIR/submm observations require the total optical depth of $\tau_B^{tot} \sim 2.6$ (Bianchi 2008) or ~ 4.0 (Popescu et al. 2000), depending on how the hidden dust component is modeled. The new submm data of Herschel/SPIRE also indicates that $\tau_B^{tot} \sim 4$ (Bianchi & Xilouris 2011). Therefore, we considered two more types of models by fixing the total optical depth $\tau_B^{tot} \equiv \tau_B^{thin} + \tau_B^{thick}$ to 2.6 (second model type) and 4 (third type). We then varied the optical depth of the thick disk τ_B^{thick} from 0.1 to 1.2 in steps of 0.05 or 0.1. Finally, the best-fit values of seven free parameters were obtained for each τ_B^{thick}: the scaleheights (z_d^{thin}, z_d^{thick} and z_s) and the maximum extents (R_d and R_s) of the dust and stellar disks, the scalelength (h_s) of the stellar disk, and the stellar luminosity. The resulting best-fit parameters versus τ_B^{thick} are shown in Figures 2 and 3 for the FUV and NUV data, respectively. In the figures, the stellar luminosities in the UV bands were converted to steady-state star-formation rates (SFRs), based on a calculation using the stellar synthesis code "starburst99" (Leitherer et al. 1999). In the calculation, the Salpeter initial mass function was adopted. z_d^{thick} and h_s for the NUV data are smaller than those of the FUV data, while z_s is larger for the NUV data. The first model type gave relatively larger values for h_s and R_d than the other types. In general, the first model type yielded slightly better fits to the data than other types. The FUV data were better reproduced than the NUV data. The maximum extent of the dust disks was always larger than that of the stellar disk. When the radial extents of the thin and thick dust disks were separately varied, the maximum extent of the thick disk was always larger than that of the thin disk. Assuming that z_d^{thin} is smaller than z_s gave a strong dust absorption lane at the galactic plane. Therefore, z_d^{thin} was always larger than z_s.

For the FUV data, the best-fits were obtained at τ_B^{thick} = 0.45, 0.5 and 0.5 in the first, second, and third model types, respectively. The best-fits for the NUV data were found at τ_B^{thick} = 0.35 regardless of the model type. However, we found that the first type models with $\tau_B^{thick} \sim 0.3-1.0$ reproduce the FUV data and the models with $\tau_B^{thick} \sim 0.2-0.9$ explain the NUV data very well. In the case of the second and third types, the models with $\tau_B^{thick} \sim 0.3-0.8$ and $\tau_B^{thick} \sim 0.25-0.5$ also matched the FUV and NUV data, respectively, very well. The

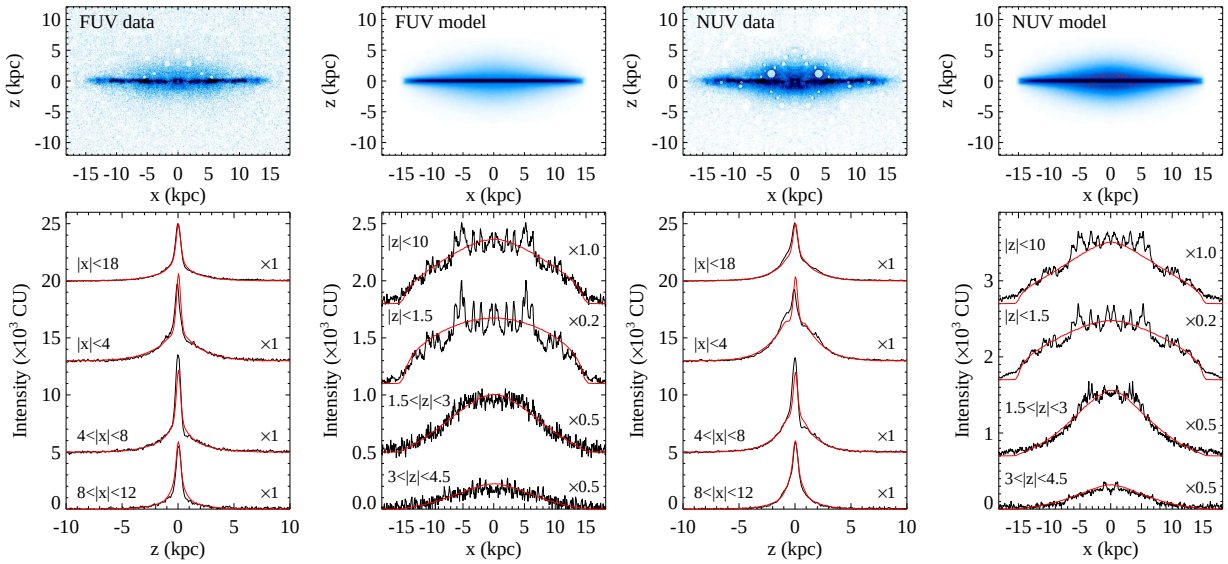

Figure 4. Comparison of the best-fit models with $\tau_B^{tot} = 2.6$ and the observed data. Two left panels show the results for the FUV data. Two right panels show the results for the NUV data. First and third columns in second row show the vertical profiles, and second and fourth columns represent the radial profiles. Red curves in the vertical and radial profile panels are the profiles of the best-fit models. Profiles were scaled by the denoted factors and shifted arbitrarily.

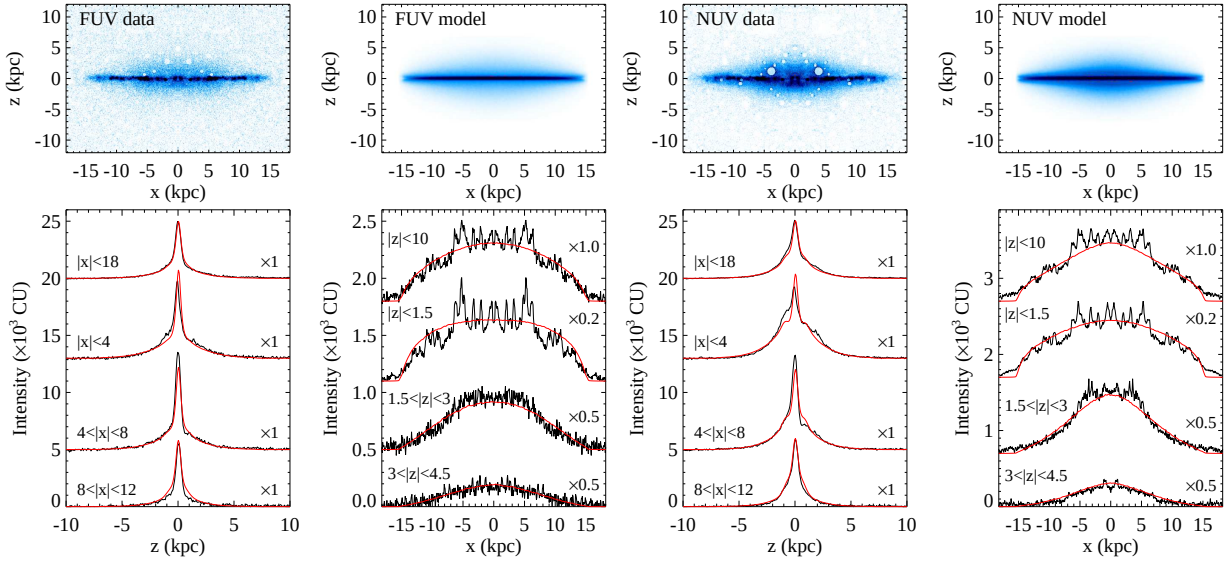

Figure 5. Same as Figure 4, but for the best-fit models with $\tau_B^{tot} = 4.0$.

optical depth of the thick disk is thus constrained to a range of $\tau_B^{thick} \approx 0.3-0.5$, as denoted by shade regions in Figures 2 and 3. We note that the scaleheight of $z_d^{thick} < 1.2$ obtained from the NUV data, as shown in Figure 3, gave relatively worse fit to the FUV data. Therefore, the same optical depth range of the thick disk is required even for the first type to explain the FUV and NUV data simultaneously.

In summary, the models with $\tau_B^{thick} \approx 0.3-0.5$, $z_d^{thick} \approx 1.2-2.0$ kpc, $z_d^{thin} \approx 0.2-0.25$ kpc, and $z_s \approx 0.08-0.10$ kpc reproduce the UV images of NGC 891 very well. Figures 4 and 5 compare the best-fit models with $\tau_B^{tot} = 2.6$ and 4.0, respectively, and the observed data. In general, the models overpredict the vertical profile in the central region ($|x| < 4$ kpc) and underpredict in the intermediate region ($4 < |x| < 8$ kpc), indicating that the real dust distribution is not smooth.

The scalelengths of stars are known to increase from the K- to the B-band in not only edge-on galaxies (Xilouris et al. 1998) but also face-on galaxies (de Jong 1996). However, the stellar scalelengths in the UV-bands are found to be smaller than those in the V- and B-bands. The stellar scalelength in the FUV band ($h_s \approx 5$ kpc) is larger than that in the NUV band ($h_s \approx 4$ kpc).

4. DISCUSSION

Two exponential (geometrically thin + thick) dust disks were needed to represent the vertically extended UV emissions of NGC 891. The optical depth of the thick dust disk was found to be $\tau_B^{thick} \approx 0.3-0.5$, corresponding to about half of the value inferred in the optical/NIR observations. We note that about half of the dust amount in the thick disk is located near the central plane ($z \lesssim 1$ kpc). Therefore, the thick disk can hide completely from the radiative transfer models of optical/NIR images when only a single dust disk is assumed.

The brightness of the UV scattered light depends not only on the amount of dust in the halo, but also on the flux of UV light coming from the galactic plane incident onto the halo.

Our models adjust the stellar luminosity such that the edge-on surface brightness of the model matches the observed surface brightness. As the optical depth of the thin disk was increased, the fraction of the UV flux incident onto the halo was decreased while the stellar luminosity was increased. Moreover, the scaleheight of the thick disk was increased, as shown in Figures 2 and 3. This resulted in a well constrained range of the optical depth of the thick disk regardless of the model type. We also note that the SFR estimated from the FUV data in the third model type is $\approx 3-4\,M_{\odot}\mathrm{yr}^{-1}$, which is consistent with the results of Popescu et al. (2000) and Bianchi (2008). However, the SFRs obtained with the NUV data are about twice higher. Better understanding on the UV halo would be obtained through radiation transfer modeling that simultaneously considers the full UV-to-submm emission from all geometrical components of dust and stellar emissivity.

The possibility of the diffuse extraplanar dust was also investigated by searching the vertically extended submm emissions in SCUBA images of NGC 891 (Alton et al. 2000a,b). Recently, Bianchi & Xilouris (2011) analyzed *Herschel*/SPIRE images of NGC 891 and placed an upper limit of ~ 1 MJy/sr on the excess emission above the galactic plane beyond that of the thin, unresolved, disk. The integrated excess emission over the effective solid angle of the halo ($\sim 4.6\times10^{-6}$ sr) is then ~ 4.6 Jy, which is about 3% of the total emission of 169 Jy at 250 μm. In our best-fit models with $\tau_{\mathrm{B}}^{\mathrm{tot}} = 4.0$, about 3−5% of the total dust mass is found in the halo above $|z| > 2$ kpc. Therefore, the present results are consistent with the submm observation.

Hodges-Kluck & Bregman (2014) investigated the possibility that the UV halos in late-type galaxies are caused by stellar populations in the halos. However, they conclude that the dust scattering nebula model is most consistent with the observations of the UV halo emission. The scaleheight of the optical polarization pattern in NGC 891 was a few kpc (Fendt et al. 1996). If only a thin dust layer is assumed, the polarization arising from scattering or dichroic extinction should be very low at high altitudes, and hence the extended polarization pattern cannot be explained (Wood & Jones 1997). Therefore, the extended optical-polarization most likely indicates the existence of a thick dust disk.

We assumed the dust properties of Milky Way dust (Draine 2003). On the other hand, Hodges-Kluck & Bregman (2014) claimed that the the halo colors and luminosities are consistent with the SMC-type dust (lacking a 2175Å UV "absorption" bump), using a simple reflection nebula model. However, the SED of the scattered flux in an optically thin environment depends only on the wavelength dependence of the scattering efficiency of the grains. Spectrophotometric studies (Andriesse et al. 1977; Calzetti et al. 1995) of the scattered light in reflection nebulae with normal to strong 2175Å features in their extinction curves have demonstrated that the 2175Å bump is a pure absorption feature, having no signature in the wavelength dependence of the scattering efficiency. Therefore, the determination of dust type in the halos does not appear possible with only the UV scattered light data. Panchromatic observations including the mid-IR (MIR) observations, together with a self-consistent radiative transfer model, may be required to determine the dust type in the halos. In fact, the vertically extended MIR continuum and PAHs emissions were also observed in the halos of NGC 891 (Burgdorf et al. 2007) and other galaxies (McCormick et al. 2013), implying the presence of the carrier of the UV absorption bump at high altitudes.

One of the promising scenarios for the origin of the extraplanar dust would be expulsion of dust in the galactic plane via stellar radiation pressure and/or (magneto)hydrodynamic flows such as galactic fountains and chimneys (Howk & Savage 1997; Greenberg et al. 1987; Ferrara et al. 1990). Hodges-Kluck & Bregman (2014) found a correlation between the UV halo luminosity and the star formation rate. A nearly linear correlation between the extraplanar PAH flux and the star formation activity in the disk was also found (McCormick et al. 2013). A large amount of dust in the intergalactic medium (IGM) was inferred from studies of dust reddening of background quasars by foreground galaxies and associated large scale structure (Ostriker & Heisler 1984; Zaritsky 1994; Aguirre et al. 2001; Menard et al. 2010). Hodges-Kluck & Bregman (2014) reported the discovery of the vertical UV halos in many spiral galaxies. The results, together with ours, suggest that the geometrically thick dust disk may be common to disk galaxies. The geometrically thick dust disk found in our study would then be an interface from which dust is ejected from spiral galaxies to the IGM.

REFERENCES

Aguirre, A., Hernquist, L., Katz, N., Gardner, J., & Weinberg, D. 2001, ApJ, 556, L11
Alton, P. B., Rand, R. J., Xilouris, E. M., et al. 2000a, A&AS, 145, 83
Alton, P. B., Xilouris, E. M., Bianchi, S., Davies, J., & Kylafis, N. 2000b, A&A, 356, 795
Andriesse, C. D., Piersma, Th. R., & Witt, A. N. 1977, A&A, 54, 841
Baes, M., Fritz, J., Gadotti, D. A., et al. 2010, A&A, 518, L39
Bianchi, S. 2008, A&A, 490, 461
Bianchi, S., & Xilouris, E. M. 2011, A&A, 531, L11
Burgdorf, M., Ashby, M. L. N., & Williams, R. 2007, ApJ, 668, 918
Byun, Y. I., Freeman, K. C., & Kylafis, N. D. 1994, ApJ, 432, 114
Calzetti, D., Bohlin, R. C., Gordon, K. D., Witt, A. N., & Bianchi, L. 1995, ApJ, 446, L97
de Jong, R. S. 1996, A&A, 313, 377
De Looze, I., Baes, M., Bendo, G. J., et al. 2012, MNRAS, 427, 2797
Draine, B. T. 2003, ApJ, 598, 1017
Fendt, C., Beck, R., Lesch, H., & Neininger, N. 1990, A&A, 308, 713
Ferrara, A., Ferrini, F., Barsella, B., & Aiello, S. 1990, A&A, 240, 259
Gil de Paz, A., Boissier, S., Madore, B. F., et al. 2007, ApJS, 173, 185
Greenberg, J. M., Ferrini, F., Barsella, B., & Aiello, S. 1982, Nature, 327, 214
Hamden, E. T., Schiminovich, D., & Seibert, M., 2013, ApJ, 779, 180
Hodges-Kluck, E., & Bregman, J. N. 2014, ApJ, submitted (arXiv:1401.4170)
Howk, J. C. & Savage, B. D. 1997, AJ, 114, 2463
Kamphuis, P., Holwerda, B. W., Allen, R. J., Peletier, R. F., & van der Kruit, P. C. 2007, A&A, 471, L1
Kuchinski, L. E., Terndrup, D. M., Gordon, K. D., & Witt, A. N. 1998, ApJ, 115, 1438
Kylafis, N. D. & Bahcall, J. N. 1987, ApJ, 317, 637
Lee, D.-H., Seon, K.-I., Min, K.-W., et al. 2008, ApJ, 686, 1155
Leitherer, C., Schaerer, D., Goldader, J. D., et al. 1999, ApJS, 123, 3
McCormick, A., Veilleux, S., & Rupke, D. S. N., 2013, ApJ, 774, 126
Ménard, B., Scranton, R., Fukugita, M., & Richards, G. 2010, MNRAS, 405, 1025
Misiriotis, A., Papadakis, I. E., Kylafis, N. D., & Papamastorakis, J. 2004, A&A, 417, 39
Misiriotis, A., Popescu, C. C., Tuffs, R., & Kylafis, N. D. 2001, A&A, 372, 775
Morrissey, P., Conrow, T., Barlow, T. A., et al. 2007, ApJS, 173, 682
Oosterloo, T., Fraternali, F., & Sancisi, R. 2007, AJ, 134, 1019
Ostriker, J. P., & Heisler, J. 1984, ApJ, 278, 1
Popescu, C. C., Misiriotis, A., Kylafis, N. D., Tuffs, R. J., & Fischera, J. 2000, A&A, 362, 138
Popescu, C. C., Tuffs, R. J., Dopita, M. A., Fischera, J., Kylafis, N. D., & Madore, B. F. 2011, A&A, 527, A109
Rand, R. J., Kulkarni, S. R., & Hester, J. J. 1990, ApJ, 352, L1

Rossa, J., Dettmar, R.-J., Walterbos, R. A. M., & Norman, C. A. 2004, AJ, 128, 674
Seon, K.-I. 2009, ApJ, 703, 1159
Seon, K.-I., Edelstein, J., Korpela, E. J., et al. 2011, ApJS, 196, 15
Seon, K.-I., & Witt, A. N. 2012, The Spectral Energy Distribution of Galaxies, Proceedings of the International Astronomical Union, IAU Symposium, Volume 284, p. 135
Seon, K.-I., & Witt, A. N. 2012, ApJ, 758, 109
Seon, K.-I., & Witt, A. N. 2013, ApJ, 778, L40
Thompson, T. W. J., Howk, J. C., & Savage, B. D. 2004, AJ, 128, 662
Tuffs, R. J., Popescu, C. C., Völk, H. J., Kylafis, N. D., & Dopita, M. A. 2004, A&A, 419, 821
van der Kruit, P. C., & Searle, L. 1981, A&A, 95, 116
Witt, A. N., Friedmann, B. C., & Sasseen, T. P. 1997, ApJ, 481, 809
Wood, K., & Jones, T. J. 1997, AJ, 114, 1405
Xilouris, E. M., Alton, P. B., Davies, J. I., Kylafis, N. D., Papamastorakis, J., & Trewhella, M. 1998, A&A, 331, 894
Xilouris, E. M., Byun, Y. I., Kylafis, N D., Paleologou, E. V., & Papamastorakis, J. 1999, A&A, 344, 868
Xilouris, E. M., Kylafis, N. D., Papamastorakis, J., Paleologou, E. V., & Haerendel, G. 1997, A&A, 325, 135
Zaritsky D., 1993, AJ, 108, 1619